Enhancement of Torque Density in Wound Field Switched Flux Machines with Partitioned Stators Using Assisted Ferrites

Zhongze Wu[1*], *Z. Q. Zhu*[2], *Shun Cai*[2], *Wei Hua*[1] *and Wentao Zhang*[1]

(1. School of Electrical Engineering, Southeast University, Nanjing 210096, China;

2. Department of Electronic and Electrical Engineering, University of Sheffield, Sheffield S10 2TN, UK)

Abstract: In this paper, ferrites are applied in a partitioned stator wound field switched flux (PS-WFSF) machine to increase the air-gap flux density, and hence, the average electromagnetic torque and overload capability. Introducing short-circuited ferrites in the inner stator in the PS-WFSF machine can increase the open-circuit phase fundamental back-EMF and average electromagnetic torque at a 60 W copper loss by 2.33% and 3.77%, respectively. Moreover, the proposed PS-WFSF machine with ferrites can exhibit a better overload capability than conventional PS-WFSF machines without ferrites, e.g., a 7.36% torque increment can be achieved when the copper loss is 120 W. The torque increment mechanism is analyzed and verified using finite element (FE) analysis. Moreover, the demagnetization of the ferrites in the proposed machine under rated on-load and overload conditions is investigated. Both prototypes of the proposed PS-WFSF machine with ferrites and a conventional one without ferrite are built and tested to validate the analytical and FE analyses.

Keywords: Average electromagnetic torque, ferrite, flux switching, partitioned stator, switched flux, torque improvement, wound field

1 Introduction

Permanent magnet (PM) machines with rare-earth materials, e.g., NdFeB, have been widely adopted in various applications, including electric and hybrid electric vehicles, owing to their high torque density and efficiency [1-3]. However, rare-earth PMs are expensive and their supply is unstable [4]. Hence, wound field (WF) synchronous machines without rare-earth PMs have recently attracted interest owing to their lower cost [4]. Wound-rotor synchronous machines contain brushes and slip rings, which are essential for DC field excitation [5]. However, they can be eliminated in wound-stator synchronous machines in which both DC and AC windings are placed in the stator while the rotor is similar to that of the switched reluctance machine [6], e.g., the WF switched flux (WFSF) machine [7-14].

A single-phase WFSF machine was proposed and analyzed in Ref. [7], and the prototype was tested as a series motor with a current source inverter. Three-phase counterparts with various topologies were analyzed in Refs. [8-10]. In Ref. [12], an analytical method based on air-gap permeance was developed for WFSF machines for a faster design. In Ref. [13] and Ref. [14], WFSF motors were developed for electric vehicles, and prototypes were built and tested. WFSF machines also have the potential to be used in generators [15-16], including high-temperature superconducting generators [17-19] and aerospace generators [20-22].

Although WFSF machines have a low cost, their limitationis also apparent in that the torque density is relatively lower than that of rare-earth PM machines. Therefore, it is important to enhance the torque density of WFSF machines. Based on the magnetic gearing effect in stator-excitation machines [23-27], a partitioned stator WFSF (PS-WFSF) machine with separated DC and AC windings in two stators was proposed and analyzed in

Manuscript received April 10, 2021; revised June 21, 2021; accepted June 30, 2021. Date of publication September 30, 2021; date of current version August 12, 2021.

* Corresponding Author, E-mail: zzwu@seu.edu.cn

Digital Object Identifier: 10.23919/CJEE.2021.000024

Ref. [28], e.g., the 12/10-stator/rotor-pole PS-WFSF machine shown in Fig. 1a. Compared with the single-stator WFSF machine analyzed in Ref. [8], the PS-WFSF machine can exhibit >19% higher torque density owing to a higher total slot area for armature windings and field winding.

In this paper, to further increase the torque density and overload capability of the 12/10-stator/rotor-pole PS-WFSF machine shown in Fig. 1a but not introduce any rare-earth PM, based on the contents reported in Ref. [29], short-circuited ferrites are applied to increase the air-gap field density (Fig. 1b).

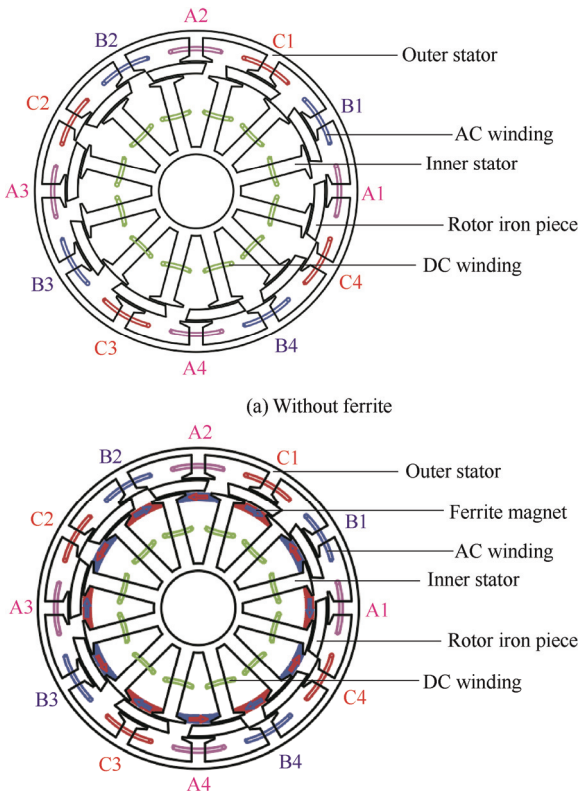

Fig. 1 Cross-sections of 12/10-stator/rotor-pole PS-WFSF machines without and with ferrites

This paper is organized as follows. Section 2 introduces the machine topologies of the proposed PS-WFSF machine with ferrites and the conventional PS-WFSF without ferrites. The torque increment mechanism is analyzed in Section 3. In Section 4, the contribution of ferrites and WF winding, as well as the armature winding, to the phase flux-linkage is analyzed using frozen permeability for open-circuit, rated on-load, and overload conditions. The demagnetization of the ferrites in the proposed machine under rated on-load and overload conditions is investigated in Section 5. Prototypes of both PS-WFSF machines with and without ferrites were built and tested for experimental validation, and they are described in Section 6. The conclusions are provided in Section 7.

2 Machine topology and specifications

The 12/10-stator/rotor-pole PS-WFSF machine without ferrites is shown in Fig. 1a, and it consists of an outer stator wound by armature windings, an inner stator wound by DC windings, and a sandwiched rotor composed of several iron pieces. The main dimensional parameters are listed in Tab. 1, which can be referred to the linear illustration shown in Fig. 2. The parameters from R_{oso} to l_{itb} in Tab. 1 are fixed, while those from R_{osy} to θ_{it} are globally optimized to achieve the largest average electromagnetic torque with a fixed total stack copper loss of p_{cu}=60 W under brushless AC (BLAC) control and zero d-axis current control, i.e., i_d=0.

Tab. 1 Main dimensional parameters of 12/10-pole PS-WFSF machines

Item	Value
Outer stator outer radius, R_{oso}/mm	45
Stack length, l_s/mm	25
Inner stator inner radius, R_{isi}/mm	10.4
Outer air-gap width, g_o/mm	0.5
Inner air-gap width, g_i/mm	0.5
Outer stator tip top length, l_{ott}/mm	0.5
Outer stator tip bottom length, l_{otb}/mm	1.5
Inner stator tip top length, l_{itt}/mm	0.5
Inner stator tip bottom length, l_{itb}/mm	1.5
Outer stator yoke radius, R_{osy}/mm	43
Outer stator inner radius, R_{osi}/mm	36.5
Rotor iron piece inner radius, R_{ri}/mm	33
Inner stator yoke radius, R_{isy}/mm	12.5
Outer stator tooth arc, θ_{ost}/(°)	6
Outer stator tip arc, θ_{ot}/(°)	4
Rotor iron piece outer arc, θ_{ro}/(°)	27
Rotor iron piece inner arc, θ_{ri}/(°)	24
Inner stator tooth arc, θ_{ist}/(°)	7
Inner stator tip arc, θ_{it}/(°)	5
PM thickness, T_{PM}/mm	2.5

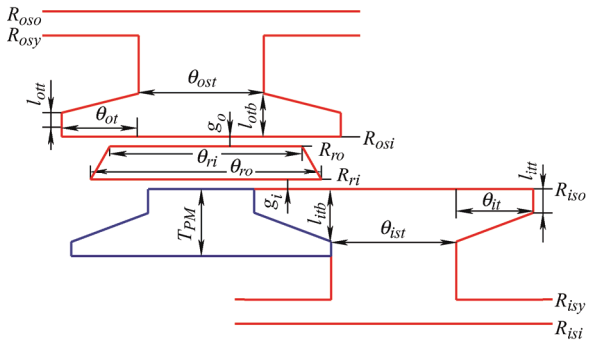

Fig. 2 Linear illustration of dimensional parameters for PS-WFSF machines without and with ferrites

The key specifications of the 12/10-pole PS-WFSF machine without ferrites are listed in Tab. 2. In Tab. 2, the efficiency η is calculated using

$$\eta = \frac{P_{out}}{P_{in}} \times 100\% = \frac{P_{EM} - p_{fe}}{P_{EM} + p_{cu}} \times 100\% \quad (1)$$

where P_{out} and P_{in} are the output and input power, respectively, P_{EM} is the electromagnetic power, and p_{fe} is the iron loss, which is calculated using

$$p_{fe} = p_{hy} + p_{ed} + p_{ex} = k_{hy} f_e B^2 + k_{ed} f_e^2 B^2 + k_{ex} f_e^{\frac{3}{2}} B^{\frac{3}{2}} \quad (2)$$

where p_{hy}, p_{ed}, and p_{ex} are the hysteresis loss, eddy current loss, and excess loss (neglected), respectively; k_{hy}=215.7 W/m^3, k_{ed}=0.35 W/m^3, and k_{ex}=0 are the corresponding coefficients for M270-35A lamination steel, respectively; f_e is the electric frequency; B is the maximum flux density.

Tab. 2 Key specifications of 12/10-pole PS-WFSF machines without and with ferrite magnets

Item	Without ferrite	With ferrites
Rated rotor speed, Ω_r/(r/min)	400	400
Rated electromagnetic torque, T_{EM}/(N • m)	1.47	1.53
Rated electromagnetic power, P_{EM}/W	61.6	64.1
Rated copper loss, p_{cu}/W	60	60
Rated iron loss, p_{fe}/W	1.28	1.44
Rated efficiency, η(%)	49.61	50.49
Rated power factor, PF	0.462	0.460

The influence of the ferrite magnet thickness on the average torque and the half-field coil slot area is investigated based on the dimensions of the PS-WFSF machine shown in Tab. 1 (Fig. 3). As shown in Fig. 3, the influence on the half-field coil slot area is significantly stronger than that on the average torque. Because ① a smaller coil area will affect the field winding copper loss and the thermal performance, and ② a small ferrite magnet thickness will affect the manufacturing and assembly of the ferrites, the ferrite magnet thickness is selected as T_{PM}=2.5 mm. Compared with the PS-WFSF machine without ferrites shown in Fig. 1a, parallel magnetized slot ferrites with a T_{PM}=2.5 mm are applied to the inner stator of the proposed PS-WFSF machine with assisted ferrites (Fig. 1b), while other machine components are the same.

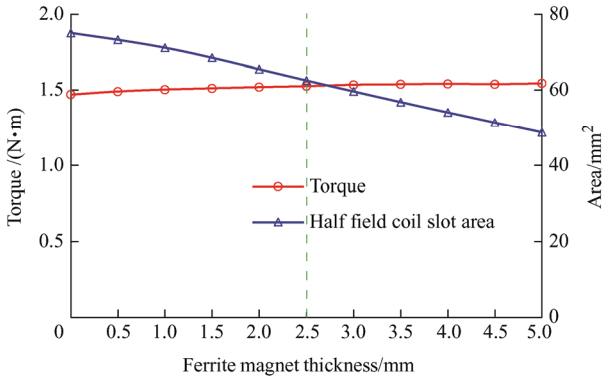

Fig. 3 Influence of ferrite magnet thickness on the average torque of the PS-WFSF machine with ferrites (BLAC, i_d=0)

3 Torque increment mechanism

As shown in Fig. 4a, the flux density B_1 can be produced in both the inner stator tooth and inner air gap owing to the WF magnetomotive force (MMF). However, an opposite flux density (B_2) can be generated in the short-circuited magnetic circuit for the ferrite MMF (Fig. 4b), while the corresponding inner air-gap flux density is B_3. Consequently, the inner air-gap flux density can be increased from B_1 in the machine without ferrites (Fig. 4a) to B_1'+B_3' in the machine with ferrites (Fig. 4c), where B_3'<B_3. Therefore, both the open-circuit phase flux-linkage and average electromagnetic torque can be increased in the proposed PS-WFSF machine with assisted ferrites. This can be evidenced by the two-dimensional (2-D) finite element (FE) predicted results shown in Fig. 5 and Fig. 6. As shown in Fig. 5, the fundamental phase flux-linkage can be increased by 2.33%, from 0.272 mWb to 0.278 mWb when the number of turns of the AC coil is N_{ac}=1.

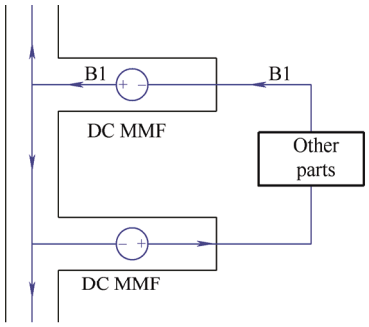

(a) WF MMF

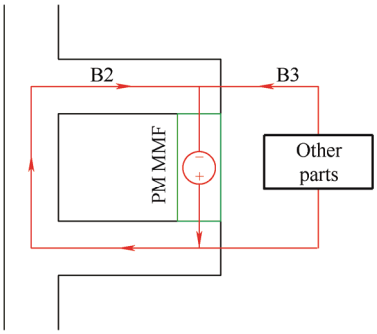

(b) Ferrite MMF

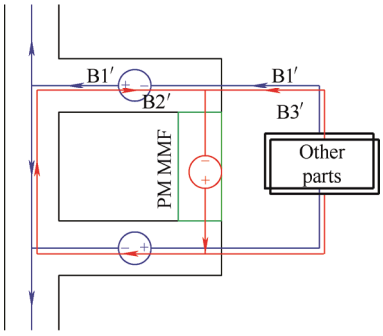

(c) WF MMF + ferrite MMF

Fig. 4 Magnetic circuit illustration for WF MMF, ferrite MMF and WF+ferrite MMF

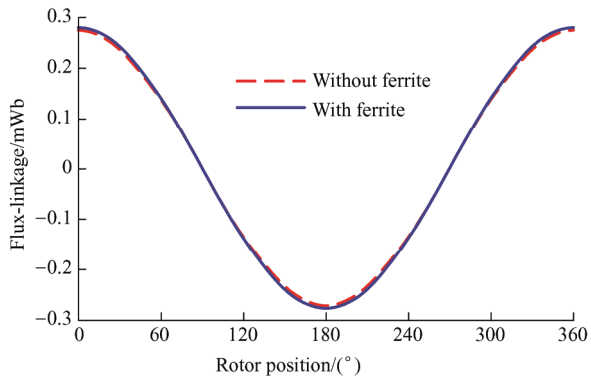

Fig. 5 Open-circuit phase flux-linkages (N_{ac}=1, p_{cuf}=30 W)

As shown in Fig. 4c, the magnetic paths of B_1' and B_2' in the inner stator are in opposite directions. This implies that the magnetic saturation of the inner stator under open-circuit conditions is lower in the machine with ferrites than that without ferrites (Fig. 7).

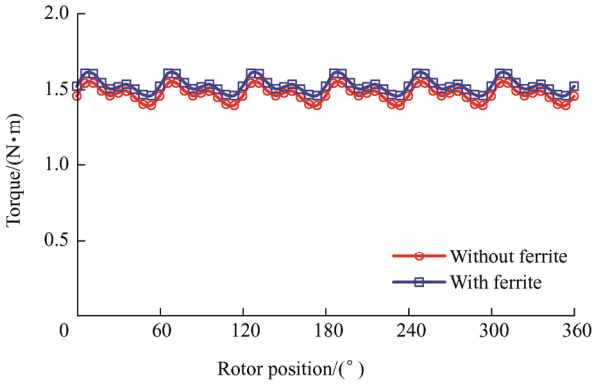

Fig. 6 On-load average torque waveforms (BLAC, i_d=0, p_{cua}=p_{cuf}=30 W)

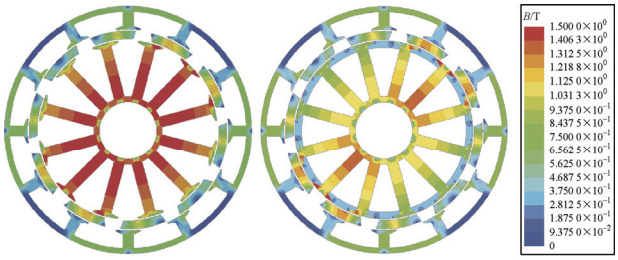

(a) Without ferrite (b) With ferrites (c) Legend

Fig. 7 Open-circuit magnetic field distribution of 12/10-pole PS-WFSF machines with and without ferrites (p_{cuf}=30 W)

Furthermore, since the on-load inner stator tooth saturation in the PS-WFSF machine without ferrites is stronger than the open-circuit one owing to armature reaction, the average electromagnetic torque can be more effectively increased by 3.77% from 1.47 N • m to 1.53 N • m, when both the DC winding copper loss (p_{cuf}) and the AC windings copper loss (p_{cua}) are 30 W and the machines operate in the BLAC mode under i_d=0, because of negligible reluctance torque [28]. Moreover, as shown in Fig. 8, a higher total copper loss and hence a stronger saturation will achieve a more effective torque improvement, i.e. a 7.36% torque increment can be achieved at a 120 W copper loss and a 9.63% torque increment can be achieved at a 240 W copper loss. This also means that the proposed PS-WFSF machine with ferrites has a better overload capability compared with the conventional PS-WFSF machine without ferrites.

The 7.36% larger average electromagnetic torque in the PS-WFSF machine with ferrites at p_{cu}=120 W is due to the higher inner air-gap flux density (Fig. 9), as well as the 9.63% larger average electromagnetic torque at p_{cu}=240 W (Fig. 4). However, the outer

air-gap flux density waveforms for the two analyzed machines are similar because the ferrites primarily affect the inner air-gap field (Fig. 9).

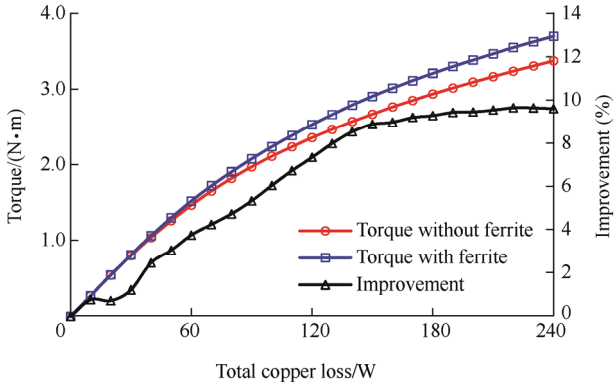

Fig. 8 Influence of total copper loss on average electromagnetic torque (BLAC, i_d=0, p_{cua}=p_{cuf})

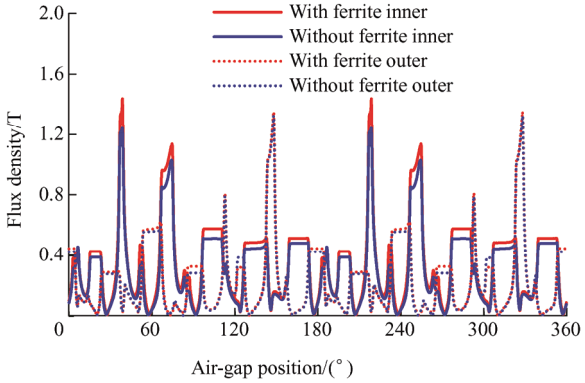

Fig. 9 Overload flux density in the inner air-gap (BLAC, i_d=0, p_{cua}=p_{cuf}=60 W)

4 Separation of AC winding flux-linkage using frozen permeability

Using frozen permeability, we can express the phase-A flux-linkage ψ_A as

$$\psi_A=\psi_A(FP,WF)+\psi_A(FP,PM)+\psi_A(FP,AR) \quad (3)$$

where ψ_A (FP, WF), ψ_A (FP, PM), and ψ_A (FP, AR) are the phase-A flux-linkages due to the WF, PM, and armature reaction (AR), respectively.

Eq. (3) can be verified using the FE predicted phase-A flux-linkage shown in Figs. 10-12 for the open-circuit, rated on-load, and overload with p_{cua}= p_{cuf}=100 W, respectively. As shown in Figs. 10-12 and Tab. 3, the ratio of the peak-to-peak value of ψ_A (FP, PM) to that of ψ_A is higher with a higher total copper loss; hence, the saturation degree is higher. This means that the ferrites in the PS-WFSF machine with ferrites are more effective with a high magnetic saturation, i.e., a higher torque increment than that without ferrites.

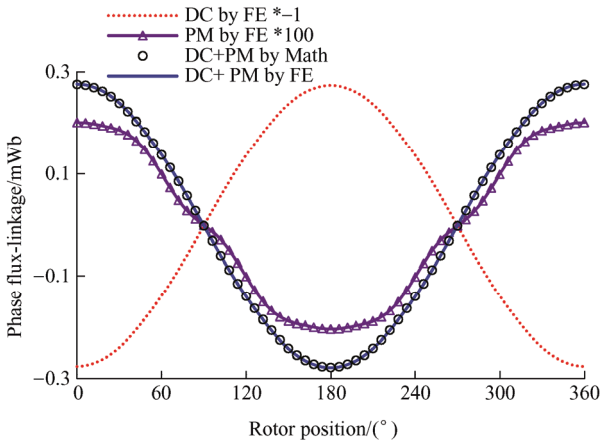

Fig. 10 Separation of open-circuit phase-A flux-linkage in the PS-WFSF machine with ferrites (N_{ac}=1, p_{cuf}=30 W)

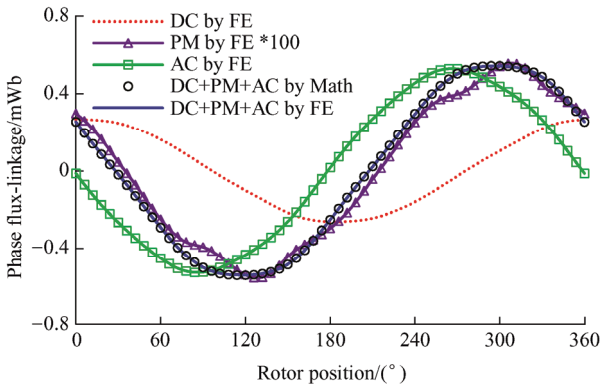

Fig. 11 Separation of rated on-load phase-A flux-linkage in the PS-WFSF machine with ferrites (BLAC, i_d=0, p_{cua}=p_{cuf}=30 W)

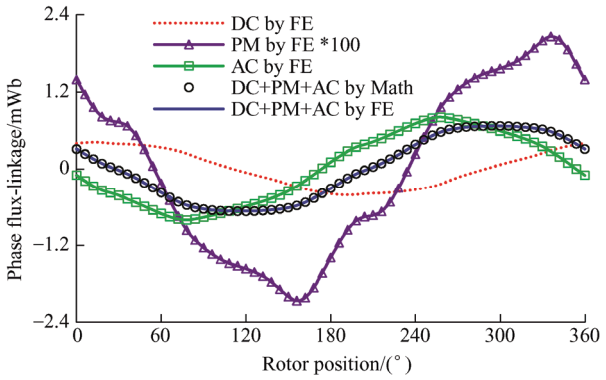

Fig. 12 Separation of rated on-load phase-A flux-linkage in the PS-WFSF machine with ferrites (BLAC, i_d=0, p_{cua}=p_{cuf}=100 W)

Tab. 3 Peak-to-peak value of phase flux-linkage in a 12/10-pole machine with ferrites using frozen permeability (N_{ac}=1)

Item	Open circuit	Rated on-load	Overload
p_{cuf}/W	30	30	100
p_{cua}/W	0	30	100
ψ_A (FP, WF)/mWb	0.550	0.531	0.831
ψ_A (FP, PM)/mWb	0.004	0.011	0.041
ψ_A (FP, AR)/mWb	—	1.057	1.614
ψ_A/mWb	0.554	1.087	1.341
ψ_A(FP, PM)/ψ_A(FP, WF) (%)	0.73	1.02	3.08

5 Demagnetization of a PS-WFSF machine with ferrites

For electrical machines using ferrites, it is important to check the demagnetization withstand capabilities under rated on-load and overload conditions [30]. Because the temperature coefficient of coercivity is positive, ferrites are more vulnerable to irreversible demagnetization at lower temperatures [30]. Consequently, an operating temperature of −20 ℃ is set as the worst condition to investigate demagnetization.

A negative i_d threatens the ferrites directly, while that of the q-axis i_q may demagnetize the PMs owing to the cross-coupling effect between the d- and q-axes [31]. Although the maximum average torque of the rated on-load condition at p_{cu}=60 W is obtained when the current angle γ=90 electric degrees with i_d=0, that for the overload conditions p_{cu}=120 W and p_{cu}=240 W is γ=100 electric degrees with i_d<0 (Fig. 13). Here, these three operating conditions, including both ratedon-load and overload were evaluated in terms of demagnetization, i.e., (p_{cu}, γ) are (60 W, 90°), (120 W, 100°), and (240 W, 100°).

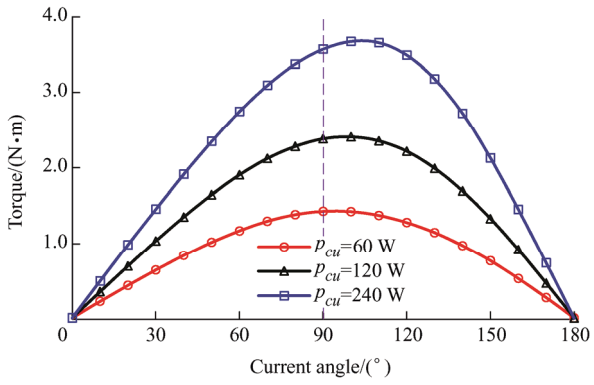

Fig. 13 Influence of current angle on average electromagnetic torque in the PS-WFSF machine with ferrites (BLAC, i_d=0, p_{cua}=p_{cuf})

In Fig. 14, the white and black areas have flux densities higher or lower than 0 T, respectively. As shown in Fig. 14, although the flux density along the magnetization direction among the major portions is higher than the demagnetization limit, i.e., 0 T, partially irreversible demagnetization will occur in the corner portions around points A and B. Therefore, six typical points are selected to investigate the influence of rotor position θ on demagnetization, i.e., points A and B and four other points C, D, E, and F close to the boundary (Fig. 14).

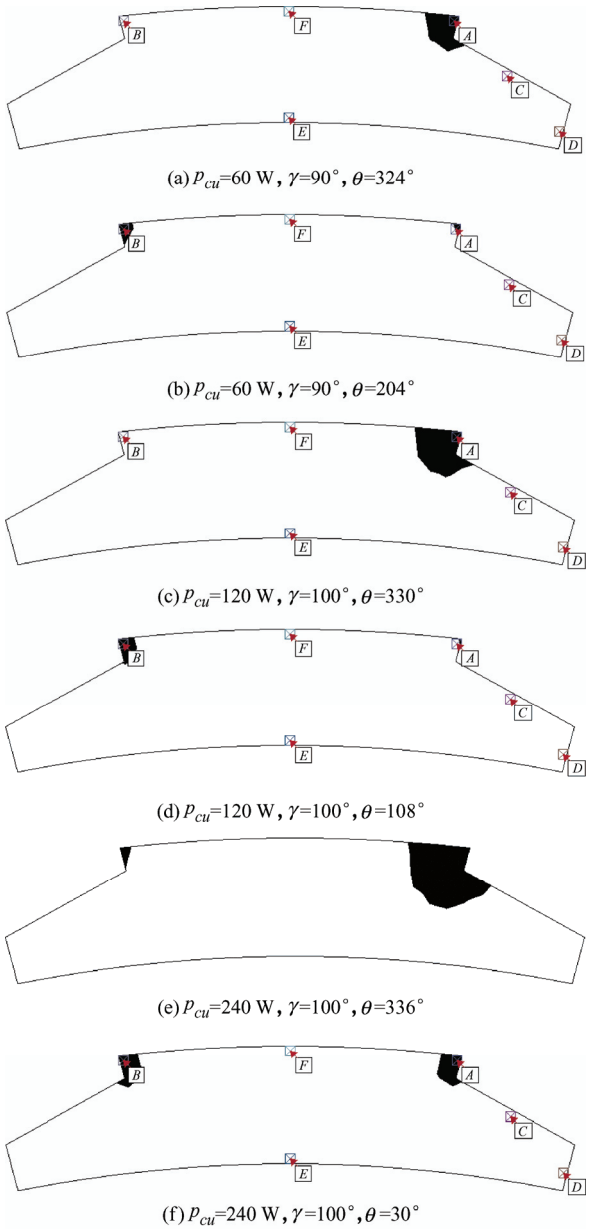

Fig. 14 Flux density distribution of ferrite PM along the magnetization direction (BLAC, p_{cua}=p_{cuf})

As shown in Fig. 15, only the corner portions around points *A* and *B*, close to the inner air gap and inner stator tooth tip, suffer from partially irreversible demagnetization for all three analyzed operation conditions. The largest area with a flux density along the magnetization direction smaller than 0 T is shown in Fig. 14 for both points *A* and *B* in all three analyzed operation conditions. Fig. 14 shows that the demagnetization area is larger with a larger load. Moreover, the area around point *D*, close to the inner stator tooth, poses a risk of demagnetization if the load is higher (Fig. 15).

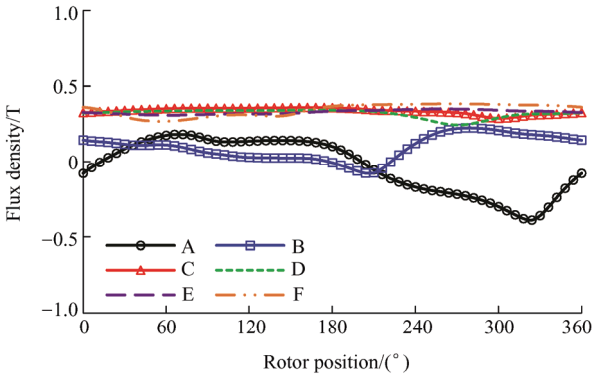

(a) P_{cu}=60 W, γ=90°

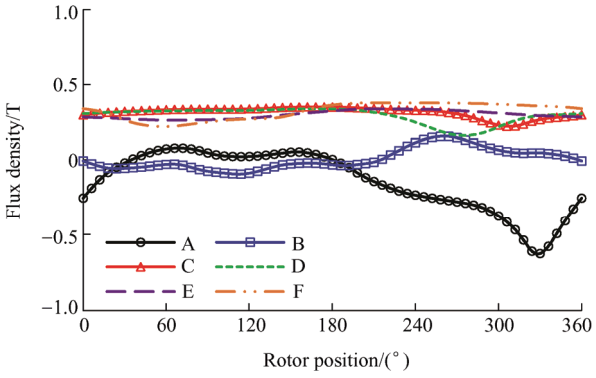

(b) P_{cu}=120 W, γ=100°

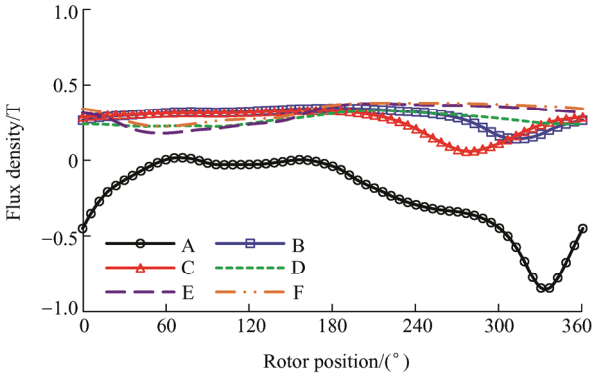

(c) P_{cu}=240 W, γ=100°

Fig. 15 Flux density of typical points along the magnetization direction versus rotor position (BLAC, p_{cua}=p_{cuf})

6 Prototypes and experimental validation

To validate the previous FE predicted results, we fabricated and tested prototypes of PS-WFSF both with and without ferrites. The two prototypes had the same outer stator and cup rotor (Fig. 16a and Fig. 16b, respectively). The inner stators of the proposed inner stator with assisted ferrites and without ferrites are shown in Fig. 16c and Fig. 16d, respectively. The main dimensional parameters of the prototypes are listed in Tab. 4, which differed slightly from those in Tab. 1 to ease manufacturing. Note that for ease of manufacturing, the rotor iron pieces were connected by T_{fb}=0.5 mm thick flux bridges, which were adjacent to the inner air gap. The open-circuit phase back-EMF and static torque under DC winding current I_f=10 A and I_f=20 A were tested, as described below.

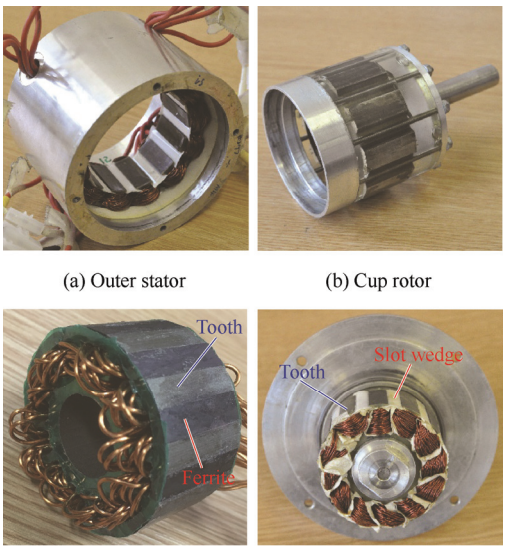

(a) Outer stator (b) Cup rotor

(c) Inner stator with ferrites (d) Inner stator without ferrite

Fig. 16 12/10-pole PS-WFSF prototype machines with and without ferrites

Tab. 4 Main dimensional parameters of the prototypes

Item	Value	Item	Value	Item	Value	Item	Value
R_{oso}/mm	45	L_{itt}/mm	0.5	R_{oso}/mm	45	L_{itt}/mm	0.5
R_{osi}/mm	31.75	L_{itb}/mm	1	R_{osi}/mm	31.75	L_{itb}/mm	1
R_{isy}/mm	15	θ_{ist}/(°)	6	R_{isy}/mm	15	θ_{ist}/(°)	6
T_{fb}/mm	0.5	θ_{it}/(°)	5.5	T_{fb}/mm	0.5	θ_{it}/(°)	5.5
g_i/mm	0.5	θ_{ri}/(°)	24	g_i/mm	0.5	θ_{ri}/(°)	24

As shown in Fig. 17, the improvement in the tested phase back-EMFs in the proposed PS-WFSF machine with ferrites was not apparent; however, they were considerably similar for the two prototypes. This

was due to the differences in dimensional parameters between the 2-D FE models and the prototypes (Tab. 1 and Tab. 4), and the introduced rotor flux bridge. However, the FE predicted open-circuit back-EMFs were validated by the experimental results for both prototypes (Fig. 17). They agreed closely with each other, although the tested results were slightly lower than those predicted using 2-D FE owing to the end effect [32]. However, as shown in Tab. 5, the measured waveforms exhibited a lower total harmonic distortion (THD) than the 2-D FE predicted waveforms in both prototypes. Here, the THD of the phase back-EMF THD_E was defined as

$$THD_E = \frac{\sqrt{E_2^2 + E_3^2 + E_4^2 \cdots}}{E_1} \tag{4}$$

where E_k (k=1, 2, 3,⋯) is the root mean square value of the k^{th} phase back-EMF harmonic.

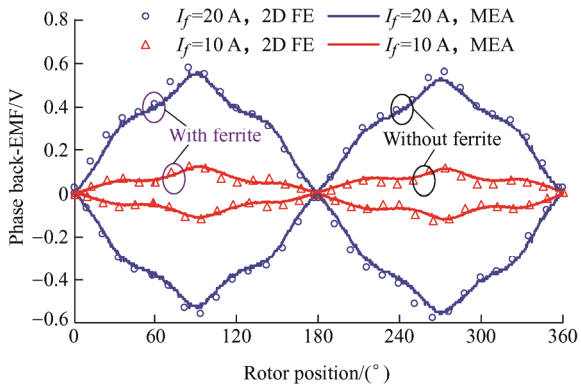

Fig. 17 Comparison of the measured and 2-D FE predicted phase back-EMF waveforms of the 12/10-pole PS-WFSF machines without and with ferrites at 400 r/min

Tab. 5 Characteristics comparison of the measured and 2-D FE predicted phase back-EMF at 400 r/min

(MEA=Measured)

Item	I_f=10 A		I_f=20 A	
	MEA	2-D FE	MEA	2-D FE
Without ferrite, E_1/V	0.09	0.08	0.47	0.50
Without ferrite, THD_E(%)	18.4	32.2	6.5	8.1
With ferrite, E_1/V	0.09	0.09	0.50	0.52
With ferrite, THD_E(%)	17.7	29.4	6.0	7.8

As shown in Fig. 18, the improvement in the tested static torques in the proposed PS-WFSF machine with ferrites was not apparent but similar for the two prototypes when I_f=10 A or I_f=20 A and I_a=10 A or I_a=20 A. This was also due to the dimensional differences between the 2-D FE models and prototypes. However, the FE predicted static torques was validated by the experimental results for both prototypes (Fig. 18 and Fig. 19). Moreover, the stronger overload capability of the PS-WFSF machine with ferrites than that without ferrites was validated by the curves shown in Fig. 19, in which the field winding current was I_f =20 A.

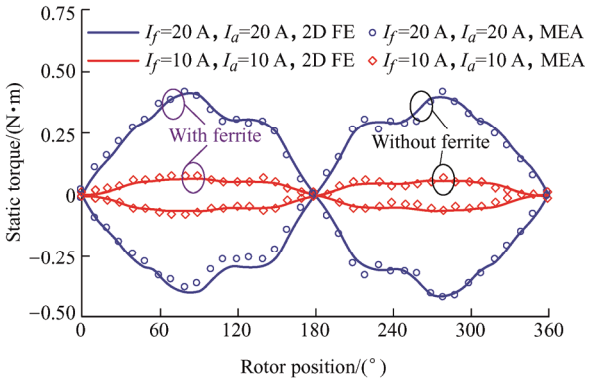

Fig. 18 Comparison ofthe measured and 2-D FE predicted static torque waveforms of the 12/10-pole PS-WFSF machines without and with ferrites

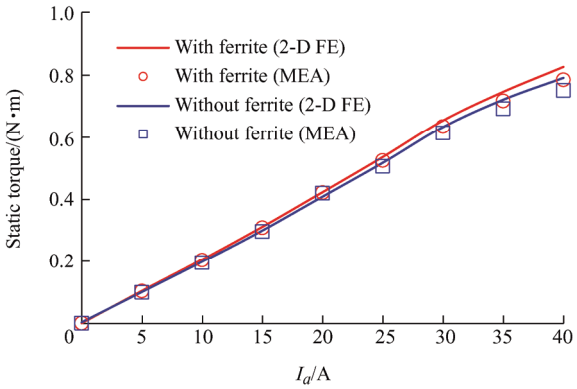

Fig. 19 Comparison of the measured and 2-D FE predicted peak static torques of the 12/10-pole PS-WFSF machines without and with ferrites (I_f=20 A)

7 Conclusions

In this study, short-circuited ferrites were applied in a PS-WFSF machine to increase the air-gap flux density and hence the average electromagnetic torque and overload capability. By introducing assisted ferrites, the open-circuit phase fundamental flux-linkage and back-EMF can be improved by 2.33%, while the rated on-load average electromagnetic torque at 60 W copper loss is increased by 3.76% owing to a more effective saturation reduction. Furthermore, a better overload

capability can be achieved in the PS-WFSF machine with ferrites, e.g., a 7.36% larger average electromagnetic torque than that without ferrites can be achieved at a 120 W copper loss. Prototypes were built, and the tested results validated the FE analysis.

References

[1] Z Q Zhu, D Howe. Electrical machines and drives for electric, hybrid and fuel cell vehicles. *Proc. IEEE*, 2007, 95(4): 746-765.

[2] M Cheng, W Hua, J Zhang, et al. Overview of stator-permanent magnet brushless machines. *IEEE Trans. Ind. Electron*., 2011, 58(11): 5087-5101.

[3] J Zheng, W Zhao, J Ji, et al. Sleeve design of permanent-magnet machine for low rotor losses. *Chinese Journal of Electrical Engineering*, 2020, 6(4): 86-96.

[4] I Boldea, L N Tutelea, L Parsa, et al. Automotive electric propulsion systems with reduced or no permanent magnets: An overview. *IEEE Trans. Ind. Electron*., 2014, 61(10): 5696-5711.

[5] M L Bash, S D Pekarek. Modeling of salient-pole wound-rotorsynchronous machines for population-based design. *IEEE Trans. Energy Convers*., 2011, 26(2): 381-392.

[6] M Ma, Z Wang, Q Yang, et al. Vector control strategy of a T-type three-level converter driving a switched reluctance motor. *Chinese Journal of Electrical Engineering*, 2019, 5(4): 15-21.

[7] C Pollock, M Wallace. The flux switching motor, a DC motor without magnets or brushes. *Conf. Rec. IEEE IAS Annu. Meeting*, 1999(3): 1980-1987.

[8] J T Chen, Z Q Zhu, S Iwasaki, et al. Low cost flux-switching brushless AC machines. *Proc. Conf. Veh. Pow. Prop.*, Lille, France, Sep., 2010: 1-6.

[9] Y Tang, J J H Paulides, T E Motoasca, et al. Flux switching machine with DC excitation. *IEEE Trans. Magn*., 2012, 48(11): 3583-3586.

[10] T Fukami, Y Matsuura, K Shima, et al. A multi-pole synchronous machine with nonoverlapping concentrated armature and field winding on the stator. *IEEE Trans. Ind. Electron.*, 2012, 59(6): 2583-2591.

[11] A Zulu, B Mecrow, M Armstrong. A wound-field three-phase flux-switching synchronous motor with all excitation sources on the stator. *IEEE Trans. Ind. Appl.*, 2010, 46(6): 2363-2371.

[12] B Gaussens, E Hoang, O de la Barrière, et al. Analytical armature reaction field prediction in field-excited flux-switching machines using an exact relative permeance function. *IEEE Trans. Magn*., 2013, 49(1): 628-641.

[13] E Sulaiman, T Kosaka, N Matsui. Design study and experimental analysis of wound field flux switching motor for HEV applications. *Proc. IEEE Inter. Conf. Elec. Mach.*, Marseille, France, Sep., 2012: 1269-1275.

[14] T Raminosoa, A M El-Refaie, D Pan, et al. Reduced rare-earth flux-switching machines for traction applications. *IEEE Trans. Ind. Appl.*, 2015, 51(4): 2959-2971.

[15] Y Wang, Z Q Deng. A position sensorless method for direct torque control with space vector modulation of hybrid excitation flux-switching generator. *IEEE Trans. Energy Convers.*, 2012, 27(4): 912-921.

[16] U B Akuru, M J Kamper. Formulation and multiobjective design optimization of wound-field flux switching machines for wind energy drives. *IEEE Trans. Ind. Electron*., 2018, 65(2): 1828-1836.

[17] X Li, S Liu, Y Wang. Design and analysis of a new HTS dual-rotor flux-switching machine. *IEEE Trans. Applied Supercon*., 2017, 27(4): 1-5.

[18] X Li, X Wang, Y Wang. Design and analysis of a new HTS linear flux-controllable doubly salient machine. *IEEE Trans. Appl. Supercond*., 2019, 29(5): 5201605.

[19] Y Wang, W Xu, X Zhang, et al. Harmonic analysis of air gap magnetic field in flux-modulation double-stator electrical-excitation synchronous machine. *IEEE Trans. Ind. Electron.*, 2020, 67(7): 5302-5312.

[20] Y Xu, Z Zhang, Z Bian, et al. Copper loss optimization based on bidirectional converter for doubly salient brushless starter/generator system. *IEEE Trans. Ind. Electron.*, 2021, 68(6): 4769-4779.

[21] W Jiang, W Huang, X Lin, et al. Analysis of rotor poles and armature winding configurations combinations of wound field flux switching machines. *IEEE Trans. Ind. Electron.*, 2021, 68(9): 7838-7849.

[22] Y Xu, Z Zhang, Z Bian, et al. Advanced angle control for active rectifier in doubly salient electromagnetic generator system. *IEEE Trans. Ind. Electron.*, 2021, 68(7): 5672-5682.

[23] M Cheng, P Han, W Hua. General airgap field modulation theory for electrical machines. *IEEE Trans. Ind. Electron*., 2017, 64(8): 6063-6074.

[24] S Jia, R Qu, J Li, et al. Principles of stator DC winding excited Vernier reluctance machines. *IEEE Trans. Energy*

Convers, 2016, 31(3): 935-946.

[25] Z Z Wu, Z Q Zhu. Analysis of air-gap field modulation and magnetic gearing effects in switched flux permanent magnet machines. *IEEE Trans. on Magn.*, 2015, 51(5): 8105012.

[26] Z Q Zhu. Overview of novel magnetically geared machines with partitioned stators. *IET Electr. Power Appl*., 2018, 12(5): 595-604.

[27] K Atallah, D Howe. A novel high-performance magnetic gear. *IEEE Trans. Magn.*, 2001, 37(4): 2844-2846.

[28] Z Q Zhu, Z Z Wu, D J Evans, et al. A wound field switched flux machine with field and armature windings separately wound in double stators. *IEEE Trans. Energy Convers*, 2015, 30(2): 772-783.

[29] Z Wu, Z Q Zhu. Torque improvement in partitioned stator wound field switched flux machine by using assisted ferrites. *Proc. Intermag.*, Singapore, Singapore, 23-27 April, 2018: 1-1. DOI: 10.1109/INTMAG.2018.8508527.

[30] S Li, Y Li, B Sarlioglu. Partial irreversible demagnetization assessment of flux-switching permanent magnet machine using ferrite permanent magnet material. *IEEE Trans. Magn*., 2015, 51(7): 8106209.

[31] G Qi, J T Chen, Z Q Zhu, et al. Influence of skew and cross-coupling on flux-weakening performance of permanent-magnet brushless AC machines. *IEEE Trans. Magn.*, 2009, 45(5): 2110-2117.

[32] Z Z Wu, Z Q Zhu. Comparative analysis of end effect in partitioned stator flux reversal machines having surface-mounted and consequent pole permanent magnets. *IEEE Trans. Magn*., 2016, 52(7): 8103904.

Zhongze Wu (S'15-M'18) received the B.E. and M.Sc. degrees in Electrical Engineering from Southeast University, Nanjing, China, in 2010 and 2013, respectively, and the Ph.D. degree in Electrical and Electronic Engineering from The University of Sheffield, Sheffield, UK, in January 2017.

Since March 2021, he has been with School of Electrical Engineering, Southeast University, Nanjing, China, as a Researcher. His major research interests include the advanced electrical machines and drives for electric propulsion systems.

From January 2017 to August 2018, he was with Warwick Manufacturing Group (WMG), University of Warwick, Coventry, UK, as a Research Fellow in electrical machines. From August 2018 to August 2020, he was with the Institute for Advanced Automotive Propulsion Systems (IAAPS), Department of Mechanical Engineering, University of Bath, Bath, UK, as a Prize Fellow, where he was a Lecturer between August 2020 and January 2021.

Z. Q. Zhu (M'90-SM'00-F'09) received the B.E. and M.Sc. degrees from Zhejiang University, Hangzhou, China, in 1982 and 1984, respectively, and the Ph.D. degree from the University of Sheffield, Sheffield, UK, in 1991, all in Electrical Engineering.

Since 1988, he has been with the University of Sheffield, where since 2000, he has been a Professor with the Department of Electronic and Electrical Engineering. He is currently the Royal Academy of Engineering/Siemens Research Chair, and the Head of the Electrical Machines and Drives Research Group, the Academic Director of Sheffield Siemens Gamesa Renewable Energy Research Centre, the Director of CRRC Electric Drives Technology Research Centre, and the Director of Midea Electrical Machines and Control Systems Research Centre. His current major research interests include the design and control of permanent magnet machines and drives for applications ranging from electrified transportation through domestic appliances to renewable energy.

Prof. Zhu is the Recipient of the 2021 IEEE Nikola Tesla Award and the 2019 IEEE IAS Outstanding Achievement Award. He is a Fellow of Royal Academy of Engineering, UK, a Fellow of Institute of Electrical and Electronics Engineers (IEEE), USA, and a Fellow of Institute of Engineering and Technology (IET), UK.

Shun Cai was born in Hubei, China. He received the B.E. and M.Sc. degrees from Zhejiang University, Hangzhou, China, in 2014 and 2017, respectively and the Ph.D. degree from the University of Sheffield, Sheffield, UK, in 2020, all in Electrical Engineering.

Since 2021, He has been a Research Fellow with Nanyang Technological University, Singapore. His research interests include design and analysis of novel permanent magnet machines for automobile application and renewable power generation.

Wei Hua (M'03-SM'16) received the B.Sc. and Ph.D. degrees in Electrical Engineering from Southeast University, Nanjing, China, in 2001 and 2007, respectively. From 2004 to 2005, he was with the Department of Electronics and Electrical Engineering, The University of Sheffield, UK, as a Joint-Supervised Ph.D. Student.

Since 2007, he has been with Southeast University, where he is currently a Chief Professor of Southeast University and a Distinguished Professor of Jiangsu Province. From 2010, he has also worked with Yancheng Institute of New Energy Vehicles of Southeast University. He has co-authored over 150 technical papers. He holds 50 patents in his areas of interest. His teaching and research interests include design, analysis, and control of electrical machines, especially for PM brushless machines and switching reluctance machines, etc.

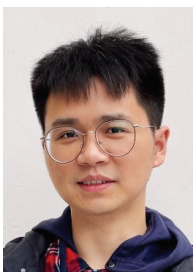

Wentao Zhang received the B.E. and M.Sc. degrees in Electrical Engineering from Southeast University, Nanjing, China, in 2018 and 2021, respectively, where he has been working toward the Ph.D. degree since September 2021.

His major research interests include the design, analysis, and control of the wound field switched flux machines.